Granuphilin molecularly docks insulin granules to the fusion machinery

Hiroshi Gomi,[1] Shin Mizutani,[1] Kazuo Kasai,[1] Shigeyoshi Itohara,[2] and Tetsuro Izumi[1]

[1]Laboratory of Molecular Endocrinology and Metabolism, Institute for Molecular and Cellular Regulation, Gunma University, Gunma 371-8512, Japan
[2]Laboratory for Behavioral Genetics, Brain Science Institute, Institute of Physical and Chemical Research, Saitama 351-0198, Japan

The Rab27a effector granuphilin is specifically localized on insulin granules and is involved in their exocytosis. Here we show that the number of insulin granules morphologically docked to the plasma membrane is markedly reduced in granuphilin-deficient β cells. Surprisingly, despite the docking defect, the exocytosis of insulin granules in response to a physiological glucose stimulus is significantly augmented, which results in increased glucose tolerance in granuphilin-null mice. The enhanced secretion in mutant β cells is correlated with a decrease in the formation of the fusion-incompetent syntaxin-1a–Munc18-1 complex, with which granuphilin normally interacts. Furthermore, in contrast to wild-type granuphilin, its mutant that is defective in binding to syntaxin-1a fails to restore granule docking or the protein level of syntaxin-1a in granuphilin-null β cells. Thus, granuphilin not only is essential for the docking of insulin granules but simultaneously imposes a fusion constraint on them through an interaction with the syntaxin-1a fusion machinery. These findings provide a novel paradigm for the docking machinery in regulated exocytosis.

Introduction

The regulated secretory pathway is highly developed in multicellular organisms and is an essential component of intercellular communication. In this pathway, bioactive substances are first stored in secretory vesicles and are released only when cells are stimulated by an external secretagogue, in contrast to the constitutive secretory pathway, where synthesized materials are continuously secreted (Burgess and Kelly, 1987). The pathway involves functionally defined sequential stages, such as movement of vesicles to the subplasmalemmal region of the cell, tethering and then docking at release sites on the plasma membrane, conversion to a fully releasable state (termed priming or maturation), triggered membrane fusion, release of vesicle contents, and finally retrieval of the vesicle membrane (Burgoyne and Morgan, 2003). Because only a subset of secretory vesicles is readily released in response to a specific stimulus in most secretory cells, distinct populations of vesicles ("pools") whose members possess distinct functional properties have been proposed (Rizzoli and Betz, 2005). However, apart from a small percentage of vesicles that are attached ("docked") to the surface membrane, the synaptic vesicles at synapses or the secretory granules in endocrine cells all look alike under the electron microscope. Furthermore, no significant biochemical distinctions that might identify different classes of vesicles are recognized. Neither has the relationship between the vesicle pools and the functional stages been sufficiently elucidated. However, there is general agreement that the secretory vesicles in a so-called readily releasable pool are probably docked and then primed for release, although the definition of the pool varies depending on the preparations and stimuli (Burgoyne and Morgan, 2003; Rorsman and Renström, 2003; Rizzoli and Betz, 2005).

To determine the significance of each functional stage, it is essential to identify its molecular basis. The concept of docking, which came from electron microscopic studies of fixed samples, remains poorly characterized on a molecular level, especially in endocrine cells that lack a morphologically specialized docking site, such as the active zone in neuronal synapses. Recent studies using evanescent wave microscopy, which allows imaging of the vesicles located in close proximity to the plasma membrane in living cells, have shown that many secretory granules in neuroendocrine cells are immobile or exhibit a severely hindered mobility and that not all of these morphologically docked granules are easily releasable (Steyer et al., 1997; Johns et al., 2001). These findings suggest the presence of an as yet unidentified molecular machinery that stably connects granules to the fusion site and simultaneously regulates their fusion.

Correspondence to Tetsuro Izumi: tizumi@showa.gunma-u.ac.jp

Abbreviations used in this paper: ADV, adenovirus; HG, high-glucose; LG, low-glucose; MOI, multiplicity of infection.

The online version of this article contains supplemental material.

The Journal of Cell Biology, Vol. 171, No. 1, October 10, 2005 99–109
http://www.jcb.org/cgi/doi/10.1083/jcb.200505179

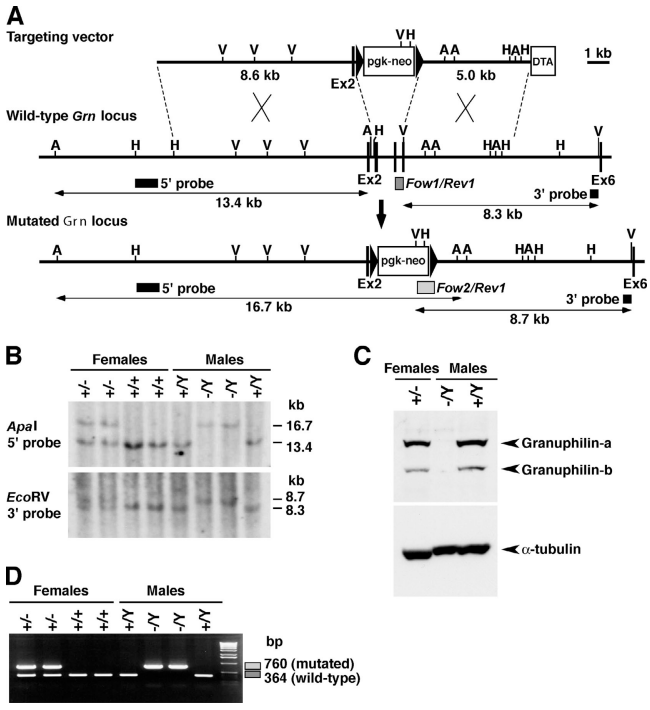

Figure 1. **Generation of *Grn* knockout mice.** (A) Targeted disruption of the granuphilin gene on mouse chromosome X. The targeting vector contains a neomycin resistance gene driven by the pgk promoter (pgk-neo) and a diphtheria toxin A fragment gene driven by the MC1 promoter (DTA) as positive and negative selection markers, respectively. Exon structures are vertically lined and partially shown from the second (Ex2) to sixth exon (Ex6). Homologous recombination results in replacement of the genomic region from the third to fifth exon with pgk-neo. A, ApaI; V, EcoRV; H, HindIII restriction sites. (B) Genomic Southern blot analysis of the backcrossed progenies from a cross of F1 female heterozygotes ($Grn^{+/-}$) with wild-type ($Grn^{+/Y}$) C3H/He male. The locations of the 5′ external probe and the 3′ external probe are shown with horizontal closed boxes in A. The 5′ probe hybridizes to a 13.4-kb ApaI fragment from the wild-type locus and to a 16.7-kb fragment from the mutated locus, and the 3′ probe hybridizes to an 8.3-kb EcoRV fragment from the wild-type locus and to an 8.7-kb fragment from the mutated locus, respectively. (C) The protein extracts from pancreatic islets were electrophoresed for immunoblotting with antigranuphilin (αGrp-N) and α-tubulin antibodies. (D) PCR genotyping of the backcrossed progenies. PCR with *Grn/Fow1*, *Grn/Rev1*, and *Neo/Fow2* mixed primers produces 364- and 760-bp fragments for wild-type and mutated alleles, respectively, as shown in boxes in A.

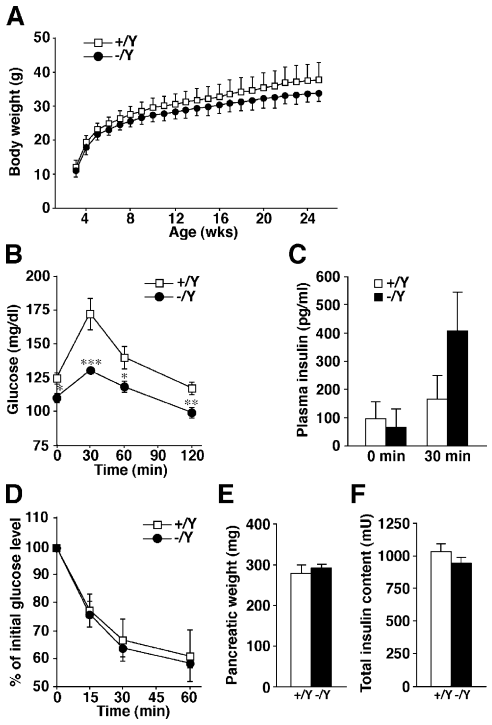

Figure 2. **In vivo phenotypes of *Grn* knockout mice.** Each measurement was performed in age-matched (8- to 33-wk-old) $Grn^{+/Y}$ (open squares or bars) and $Grn^{-/Y}$ (closed circles or bars) male mice. (A) Body weight change after the weaning (mean ± SD). (B) Blood glucose concentrations during an i.p. glucose tolerance test ($n = 11$ for $Grn^{+/Y}$ mice; $n = 13$ for $Grn^{-/Y}$ mice). *, $P < 0.05$; **, $P < 0.01$; ***, $P < 0.002$. (C) Plasma insulin concentrations before and 30 min after a glucose load ($n = 8$ for 0 min; $n = 9$ for 30 min). (D) Percentage of starting blood glucose concentration during an i.p. insulin tolerance test ($n = 5$ for $Grn^{+/Y}$ mice; $n = 6$ for $Grn^{-/Y}$ mice). Pancreatic weight (E) and total insulin content in the pancreas (F) of 20-wk-old $Grn^{+/Y}$ and $Grn^{-/Y}$ mice ($n = 6$). Results are provided as mean ± SEM.

We propose that granuphilin is a plausible candidate molecule that meets the criteria for docking machinery in regulated exocytosis. Granuphilin was originally identified as a gene product that is preferentially expressed in pancreatic β cells (Wang et al., 1999). It physiologically interacts with the small GTPase Rab27a (Yi et al., 2002), although it also shows an affinity to Rab3a in vitro and by yeast and mammalian two-hybrid assay (Coppola et al., 2002; Yi et al., 2002). In addition, granuphilin directly binds to the plasma membrane–anchored SNARE syntaxin-1a (Torii et al., 2002) and to Munc18-1 (Coppola et al., 2002). Overexpression of granuphilin in β cell lines decreases evoked exocytosis (Coppola et al., 2002; Torii et al., 2002) and redistributes insulin granules to the peripheral area close to the plasma membrane (Torii et al., 2004). The latter finding suggests that granuphilin regulates exocytosis at the docking stage. In this study, we investigated the role of granuphilin in insulin secretion using a reverse genetic approach and demonstrated that the number of insulin granules morphologically docked to the plasma membrane was markedly reduced in granuphilin-deficient β cells. The docking defect, however, did not result in a decrease of evoked insulin secretion but instead caused its increase. Rescue experiments indicated that the docking-promoting activity of granuphilin required its interaction with syntaxin-1a. Our findings have begun to elucidate the docking machinery of insulin granules and indicate that molecular docking is not a prerequisite but a temporal brake for subsequent fusion. This view provides a novel paradigm for the docking–fusion coupling machinery that underlies the core nature of regulated exocytosis, where constitutive fusion of incoming vesicles is inhibited.

Results

Generation and in vivo phenotypes of granuphilin-null mice

To study the cellular function of granuphilin, we generated a mouse line lacking granuphilin using the gene knockout approach (Fig. 1). The granuphilin gene (*Grn*) is mapped on the X chromosome and therefore is present as a single copy in male mice. Mice heterozygous for the targeted allele in the female ($Grn^{+/-}$) were obtained by crossing the male chimeras

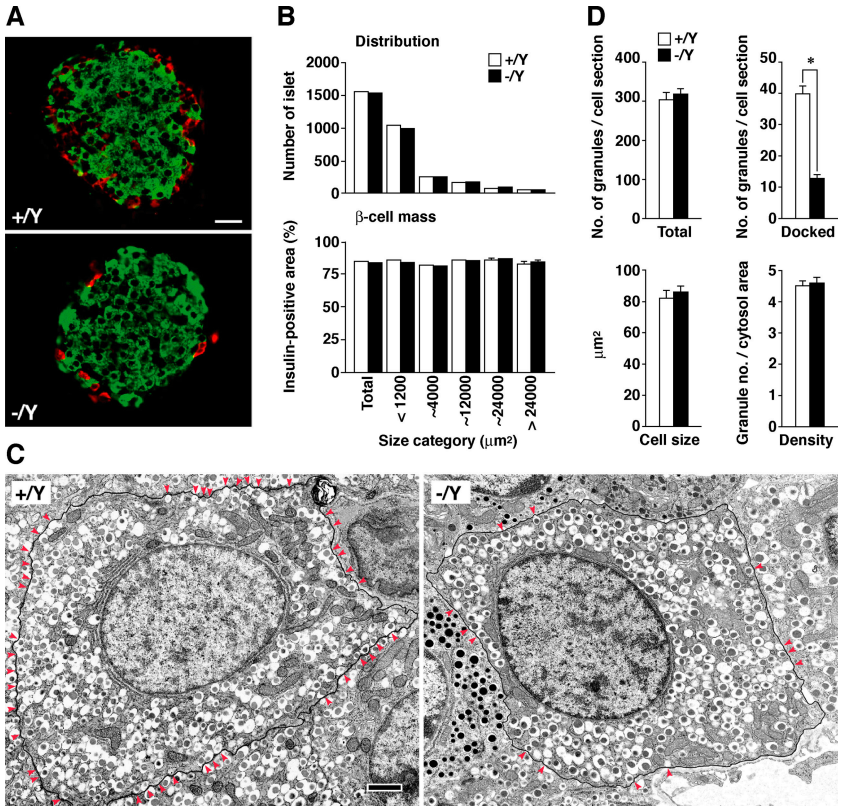

Figure 3. **Microscopic inspection of pancreatic islets.** (A) Immunofluorescent detection of insulin (green) and glucagon (red) in frozen sections (20 μm) of pancreas. Bar, 20 μm. (B) Morphometric analyses of islet size distribution and β cell mass. Total numbers of islets analyzed were 1,533 from three $Grn^{+/Y}$ mice (open bars) and 1,510 from three $Grn^{-/Y}$ mice (closed bars). (C) The numbers of total and docked insulin granules per single β cell section, the β cell size, and the granule density (granule number/cytosol area) in ultrathin sections (90 nm). 21 β cells were analyzed from each of three 12- to 20-wk-old male $Grn^{+/Y}$ (open bars) and $Grn^{-/Y}$ mice (closed bars). *, $P < 0.0001$. (D) Electron micrographs of pancreatic tissue section. The plasma membrane of a single β cell is framed with a black line, and docked granules whose contours touch the plasma membrane are marked by red arrowheads. Bar, 1 μm. Results are provided as mean ± SEM.

with female C3H/He mice ($Grn^{+/+}$). Mutant ($Grn^{-/Y}$) and control wild-type ($Grn^{+/Y}$) male mice for the experiments were obtained by backcrossing the female $Grn^{+/-}$ mice with male C3H/He mice. In the wild-type mouse islets, granuphilin-a was predominantly expressed relative to the granuphilin-b isoform (Fig. 1 C), in contrast to the roughly equal expression of the two isoforms in the cultured β cell line MIN6 (Yi et al., 2002). Immunoblot and immunofluorescent analyses confirmed the absence of granuphilin-a and -b in the pancreatic β cells of the $Grn^{-/Y}$ mice (Fig. 1 C and not depicted).

We first examined in vivo the phenotypes that might be affected by potential insulin secretion defects. Granuphilin-null male mice showed normal development and were fertile, with no apparent abnormalities in general appearance or behavior. However, their weight showed a reduction of ~10% at all ages examined (Fig. 2 A), which may be related to the mild growth defect seen in loss-of-function mutants of bitesize, the *Drosophila melanogaster* granuphilin homologue (Serano and Rubin, 2003). We found that the blood glucose levels examined in fasting mice or after a glucose load were significantly lower in mutant mice (Fig. 2 B). Plasma insulin concentrations after a glucose load were slightly but not significantly higher (Fig. 2 C), although it is generally difficult to measure them accurately from a limited sample size in mice. Insulin tolerance tests showed comparable insulin sensitivity between the mutant and control mice (Fig. 2 D). There was no change in the pancreas tissue weight or in the total insulin content (Fig. 2, E and F). These findings indicate that granuphilin-null mice have enhanced glucose tolerance without signs of increased insulin sensitivity in peripheral tissues.

Microscopic inspection of pancreatic islets

We performed morphological analyses of the pancreatic islets. Insulin and glucagon double immunofluorescent labeling showed a typical mantle structure between the α and β cells in the mutant islets (Fig. 3 A). Morphometric analysis on paraffin-embedded pancreatic tissue sections that had been immunostained with antiinsulin antibody revealed that the number and size distribution of the islets and the β cell mass in the sized islets were not different between the mutant and control tissues (Fig. 3 B). However, the ultrastructure of the mutant β cells showed a deficit in insulin-granule docking at the plasma membrane (Fig. 3 D). The number of docked granules was significantly reduced in the granuphilin-null β cells (40 vs. 13 in control and mutant β cells, respectively; $P < 0.0001$), whereas the granule number per cell section, the β cell size, and the average granule density were unchanged (304 vs. 319 granule number, 82.1 vs. 86.1 μm^2 cell size, 4.5 vs. 4.6 granules per μm^2 cytosol area of control and mutant β cells, respectively; Fig. 3 C).

Insulin secretion from perifused islets

To examine whether the reduced number of docked granules affects the insulin secretion ability, we performed perifusion analyses in isolated islets. In the granuphilin-null islets, insulin secretion in response to 16.7 mM glucose was significantly enhanced in both the first and second phases, by ~200% of the control levels ($P < 0.05$; Fig. 4 A), although the peak of first-phase secretion was delayed by ~4 min. The increase of insulin secretion was observable after repeated exposure to high concentrations of glucose but became less evident with later

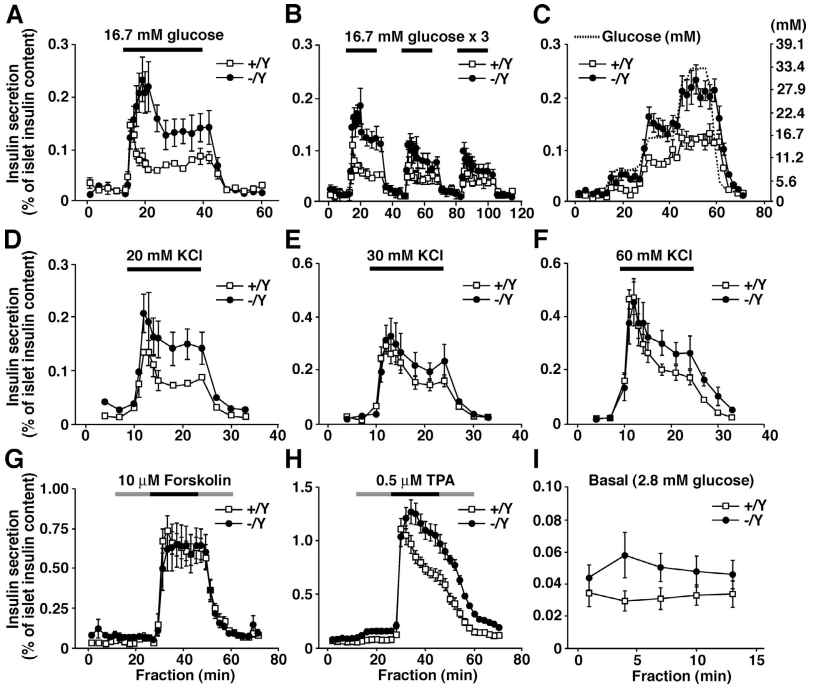

Figure 4. **Insulin secretion profiles in perifused islets.** Islets isolated from age-matched (15- to 20-wk-old) male $Grn^{+/Y}$ (open squares) or $Grn^{-/Y}$ (closed circles) mice were perifused with standard LG (2.8 mM) Krebs-Ringer buffer for 30 min. Thereafter, the collection of each fraction (1 ml/min) was started, and an appropriate secretagogue was applied 10 min after the start. (A) Single stimulation by HG buffer. Islets were perifused with 16.7 mM glucose buffer for 30 min (horizontal black line) followed by 2.8 mM glucose buffer for 20 min ($n = 5$). (B) Repeated stimulation by 16.7 mM glucose buffer for 20 min ($n = 4$). (C) Stimulation by graded increase of glucose concentrations (dashed line) from 2.8 to 7.8, 16.7, and 33.4 mM each for 15 min ($n = 6$). (D–F) Depolarizing stimulation by high K^+ buffer containing 20 mM KCl and 105 mM NaCl (D), 30 mM KCl and 95 mM NaCl (E), or 60 mM KCl and 65 mM NaCl (F) for 15 min ($n = 5$). (G and H) Application of 10 μM forskolin (G; $n = 6$) or 0.5 μM phorbol-12-myristate-13-acetate (H; $n = 9$). In the continuous presence of either drug (black and gray lines), islets were stimulated by 16.7 mM glucose buffer for 20 min (black line), with pre- and postincubation stimulation of 2.8 mM glucose buffer for 15 min (gray line). (I) Basal secretion. Data for the secretion at 2.8 mM glucose before the application of secretagogues in panels A–C, G, and H are combined ($n = 30$). Results are provided as mean ± SEM.

stimuli (Fig. 4 B). Stimulation by graded increases of glucose concentrations again showed a higher insulin response ($P < 0.003$) but no significant change in glucose sensitivity (Fig. 4 C). Depolarization by a high KCl concentration (20 mM) also evoked stronger insulin release in the mutant islets ($P < 0.005$; Fig. 4 D). The application of a higher KCl concentration (30 and 60 mM) induced similar but not statistically significant increases (Fig. 4, E and F). Although the effect of forskolin (an activator of adenylate cyclase) in the presence of high glucose was indistinguishable between the mutant and control islets (Fig. 4 G), phorbol-12-myristate-13-acetate (a PKC activator) enhanced the release of insulin in the mutant islets ($P < 0.002$; Fig. 4 H). The differential effects of each secretagogue likely reflect differences in its mode of granule recruitment for fusion. Overall, in our experiments, the basal secretion was slightly but not significantly increased in the granuphilin-deficient islets (Fig. 4 I). The observed enhancement of insulin secretion in response to physiological or some nonphysiological stimuli in the granuphilin-null β cells is consistent with previous findings that the overexpression of granuphilin in cultured β cell lines profoundly inhibits stimulus-induced secretion (Coppola et al., 2002; Torii et al., 2002). Therefore, granuphilin plays a negative regulatory role in secretagogue-evoked insulin secretion.

Morphometric analyses of insulin-granule docking in isolated islets

Torii et al. (2004) showed that the overexpression of granuphilin in MIN6 cells induces a redistribution of insulin granules to the peripheral plasma membrane area. Thus, in the present study we performed a detailed electron microscopic analysis in isolated islets. The islets were incubated with either a low-glucose (LG) or a high-glucose (HG) buffer and fixed in the fixative (Fig. 5, A and B). The insulin granules were categorized into six bins according to their distance from the granule center to the plasma membrane, and the relative density of granules in each bin was calculated. The density of granules with centers that resided within 100 nm of the plasma membrane (first bin) was much lower than the average granule density in the cytoplasm (i.e., 100%; Fig. 5 C), which is not surprising considering that the diameter of insulin granules is ∼350 nm (Kasai et al., 2005; also see the end of this paragraph). By contrast, the density of the granules with centers that resided at 100–200 nm (second bin) was markedly greater than the average for the wild-type cells, which indicates an accumulation of granules docked to the plasma membrane, as reported previously (Kasai et al., 2005). The densities of the granules in both fractions were drastically reduced in the granuphilin-null β cells irrespective of the preincubated glucose concentrations (for granules within 0–100 nm, 10.2 ± 3.2% and 7.1 ± 2.0% in LG- and HG-treated control cells, respectively, vs. 1.6 ± 1.1% and 1.9 ± 1.2% in LG- and HG-treated mutant cells, respectively; for granules within 100–200 nm, 182.5 ± 23.2% and 219.4 ± 21.9% in LG- and HG-treated control cells, respectively, vs. 60.0 ± 10.9% and 63.8 ± 9.4% in LG- and HG-treated mutant cells, respectively). By contrast, the relative densities of the granules within 300–400 nm (fourth bin) and at >500 nm (sixth bin) were significantly increased (for granules within 300–400 nm, 87.2 ± 8.0% and 81.9 ± 3.7% in LG- and HG-treated control cells, respectively, vs. 144.0 ± 8.3% and 123.1 ± 11.0% in LG- and HG-treated mutant cells, respectively; for granules at >500 nm, 91.7 ± 4.0% in HG-treated control cells vs. 104.3 ± 1.2% in HG-treated mutant cells). Although the mean granule diameter was slightly larger in the mutant β cells (324.9 and 339.4 nm in LG- and HG-treated

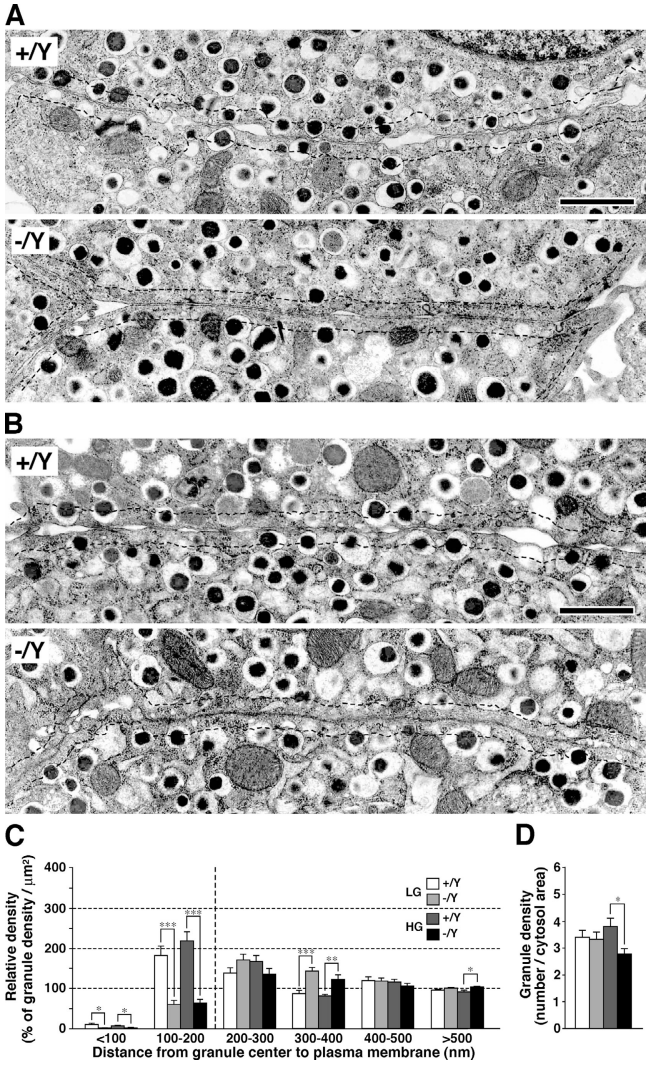

Figure 5. **Granule docking in isolated islets.** (A and B) Electron micrographs of β cell sections. Islets were isolated from 24-wk-old male *Grn*$^{+/Y}$ and *Grn*$^{-/Y}$ mice and incubated at 37°C with 2.8 mM LG buffer for 1 h (A) and then with 25 mM HG buffer for 30 min (B). Dashed lines indicate a border 200 nm distant from the plasma membrane. Bars, 1 μm. (C and D) Morphometric analyses of insulin granules in LG-treated *Grn*$^{+/Y}$ (white bars) and *Grn*$^{-/Y}$ islets (light gray bars), and HG-treated *Grn*$^{+/Y}$ (dark gray bars) and *Grn*$^{-/Y}$ islets (black bars). For each group, 10 randomly selected β cells from four different animals were analyzed. (C) Relative density of insulin granules located near the plasma membrane. The granules were categorized into six bins according to their distance from the granule center to the plasma membrane (nm). The data were represented as a percentage of the granule density in each bin (100% corresponds to the average granule density in cytoplasm). *, $P < 0.05$; **, $P < 0.005$; ***, $P < 0.0003$. (D) Average granule number per cytosol area (μm²). *, $P = 0.012$. Results are provided as mean ± SEM.

control cells, respectively, vs. 345.7 and 377.6 nm in LG- and HG-treated mutant cells, respectively; $P < 0.001$), these 6–11% changes should not affect the granule locations. The mean granule density was significantly decreased in the HG-treated mutant β cells (3.81 ± 0.31 in control cells vs. 2.80 ± 0.19 in mutant cells; Fig. 5 D), which could be related to the enhanced insulin secretion. These results strongly indicate that granuphilin is essential for the docking of insulin granules to the plasma membrane.

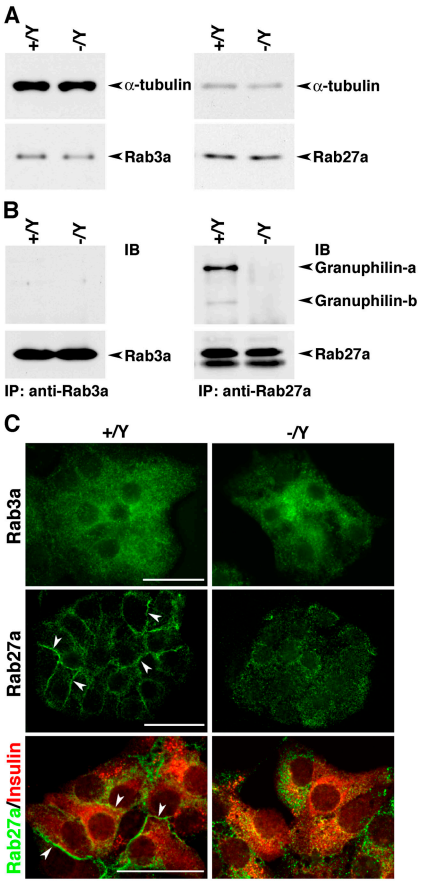

Figure 6. **Expression and intracellular distribution of granuphilin-binding Rab3a and -27a.** (A) Immunoblot analysis of Rab3a, Rab27a, and α-tubulin in total lysates from *Grn*$^{+/Y}$ and *Grn*$^{-/Y}$ islets. (B) Coimmunoprecipitation of granuphilin in the Rab3a or -27a immunoprecipitates. Protein from 400–600 islets was extracted with 1% Triton X-100–containing lysis buffer and immunoprecipitated (IP) with anti-Rab3a or anti-Rab27a antibodies followed by immunoblotting (IB) with antigranuphilin αGrp-N and anti-Rabs antibodies. (C) Immunofluorescent labeling of Rab3a, Rab27a, and insulin in the islet monolayer culture. Rab27a is diffusely dispersed of in *Grn*$^{-/Y}$ cells in contrast to the marginal distribution in *Grn*$^{+/Y}$ cells (arrowheads). Bars, 25 μm.

Analyses of granuphilin-interacting proteins in pancreatic β cells

To explore the molecular mechanism that underlies these phenotypes, we investigated the granuphilin-interacting proteins. Because granuphilin can bind to both Rab27a and -3a in vitro (Coppola et al., 2002; Yi et al., 2002), we examined the effect of granuphilin deletion on the expression and cellular localization of these Rab proteins. The expression level of either Rab27a or -3a was not affected by loss of granuphilin (Fig. 6 A and see Fig. S1, available at http://www.jcb.org/cgi/content/full/jcb.200505179/DC1, for the entire images of immunoblots). Consistent with our previous findings in MIN6 cells (Torii et al., 2002; Yi et al., 2002), coimmunoprecipitation assays demonstrated the preferential interaction of granuphilin with Rab27a in wild-type islets, whereas the interaction with Rab3a was barely detectable (Fig. 6 B). Although we could not detect changes in the distribution pattern in the pancreatic islet sections (unpublished data), we observed a marked redistribution

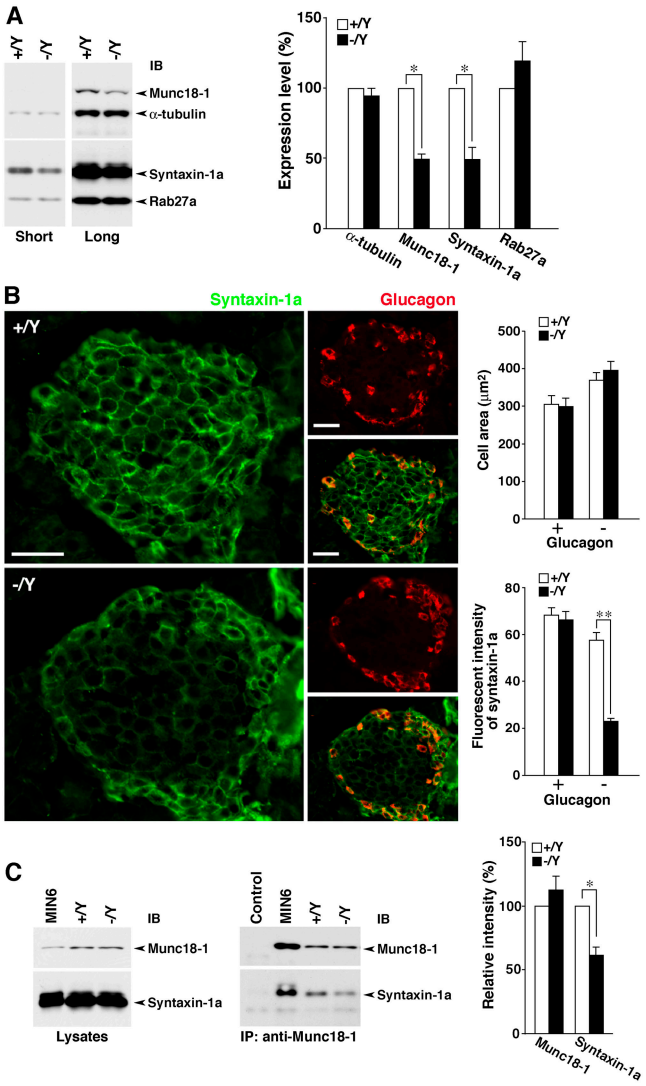

Figure 7. **Expression and complex formation of granuphilin-interacting syntaxin-1a and Munc18-1 in islets.** (A) Expression levels of syntaxin-1a and Munc18-1 in islets. Islet protein was extracted by homogenization with 1× SDS sample buffer and the equivalent amount from 16 to 20 islets was loaded per lane. Protein-transferred membranes were separated into upper and lower parts at the region representing a molecular mass of ~45 kD and then reacted with anti–Munc18-1/anti–α-tubulin (upper) and anti–syntaxin-1a/anti-Rab27a (lower) antibody mixtures. Signals with short- and long-term exposure in immunoblots (IB) reveal the decreased levels of syntaxin-1a and Munc18-1 in $Grn^{-/Y}$ islets, respectively (left). Protein expression levels in $Grn^{+/Y}$ (open bars) and $Grn^{-/Y}$ islets (closed bars) were quantified from seven experimental preparations (right). *, $P = 0.018$. (B) Immunofluorescent analysis of syntaxin-1a (green) and glucagon (red) in frozen pancreatic tissue sections. The syntaxin-1a immunosignal is specifically reduced in the glucagon-negative cells mainly located in the center area of the islet. Bars, 50 μm (left). The cell area (μm²) and the immunofluorescent intensity of syntaxin-1a were quantified for glucagon-positive (+) and -negative (−) islet cells ($n = 15$) of $Grn^{+/Y}$ (open bars) and $Grn^{-/Y}$ mice (closed bars; right). **, $P < 0.0001$. (C) The complex formation between syntaxin-1a and Munc18-1. The sample lysates for immunoprecipitation were prepared with 1% Triton X-100–containing buffer, and the amounts of Munc18-1 and syntaxin-1a were adjusted equally between $Grn^{+/Y}$ and $Grn^{-/Y}$ islets (left). These and MIN6 cell lysates were immunoprecipitated with anti–Munc18-1 serum. In the control lane, MIN6 cell extracts were immunoprecipitated with normal rabbit serum. The immunoprecipitates (IP) were analyzed by immunoblotting with anti–Munc18-1 and anti–syntaxin-1a mAb (middle). Relative intensities of signals in $Grn^{-/Y}$ islets (closed bars) to those in $Grn^{+/Y}$ islets (open bars) were calculated from six independent experiments (right). *, $P = 0.027$. Results are provided as mean ± SEM.

of Rab27a, but not of Rab3a, in the monolayer β cells (Fig. 6 C). Compared with the marginal distribution to the plasma membrane in control cells, Rab27a was diffusely dispersed in the cytoplasm of the granuphilin-deficient cells. These results strongly support our previous proposals that Rab27a is a physiologically dominant granuphilin-binding Rab protein in vivo (Torii et al., 2002; Yi et al., 2002; Kasai et al., 2005).

Besides Rab27a, granuphilin directly binds to the plasma membrane–anchored SNARE protein syntaxin-1a, and this interaction is positively regulated by Rab27a (Torii et al., 2002). Granuphilin has also been shown to bind to Munc18-1 in vitro and in a mammalian two-hybrid assay (Coppola et al., 2002). It was, however, very difficult to detect the endogenous protein complex between granuphilin and Munc18-1 in the islets using coimmunoprecipitation (unpublished data). Further, the amount of Munc18-1 in the granuphilin immunoprecipitates is highly correlated with the amount of coprecipitated syntaxin-1a in MIN6 cells, as previously reported (Torii et al., 2002). Because Munc18-1 itself interacts with syntaxin-1a (Dulubova et al., 1999; Misura et al., 2000; Yang et al., 2000), it is currently unknown whether granuphilin forms a complex with Munc18-1 directly or through syntaxin-1a. The expression levels of syntaxin-1a and Munc18-1 were profoundly diminished by ~50% in the mutant islets (49.4 ± 8.7% for syntaxin-1a and 49.5 ± 3.6% for Munc18-1; $P = 0.018$), although those of α-tubulin and Rab27a were not significantly different (94.5 ± 5.7% for α-tubulin and 119.6 ± 13.7% for Rab27a; Fig. 7 A and Fig. S1). Remarkably, immunofluorescent analysis demonstrated that the decrease of syntaxin-1a expression was specific to the glucagon-negative, deducible β cells (Fig. 7 B), where granuphilin is specifically expressed in normal islets (Wang et al., 1999), indicating an even more severe reduction in β cells. We then examined the complex formation between Munc18-1 and syntaxin-1a. Because the expression levels of both proteins are reduced in mutant islets, we adjusted the amount of lysate proteins equally between the control and mutant samples for the coimmunoprecipitation experiments (Fig. 7 C). Although the amount of Munc18-1 in its immunoprecipitate was similar, the amount of coprecipitated syntaxin-1a was significantly reduced in the mutant islets (112.0 ± 10.5% for Munc18-1 and 61.0 ± 6.2% for syntaxin-1a of the control; $P = 0.027$). The impairment of the complex formation in physiological cells should be more severe without the adjustment of protein levels. These results indicate that granuphilin is essential both for the preservation of expression levels of syntaxin-1a and Munc18-1 and for the maintenance of the syntaxin-1a–Munc18-1 complex formation.

Adenovirus (ADV)-mediated granuphilin expression in granuphilin-null β cells

We performed rescue experiments to examine whether defects in granuphilin-deficient β cells are reversibly and specifically restored by the expression of exogenous granuphilin. We first examined the optimum infective condition using ADV-encoding β-galactosidase (LacZ) to probe the infection efficiency in isolated islets (Fig. 8 A). Although LacZ expression was weak and inhomogeneous in the islet cells at a multiplicity of infec-

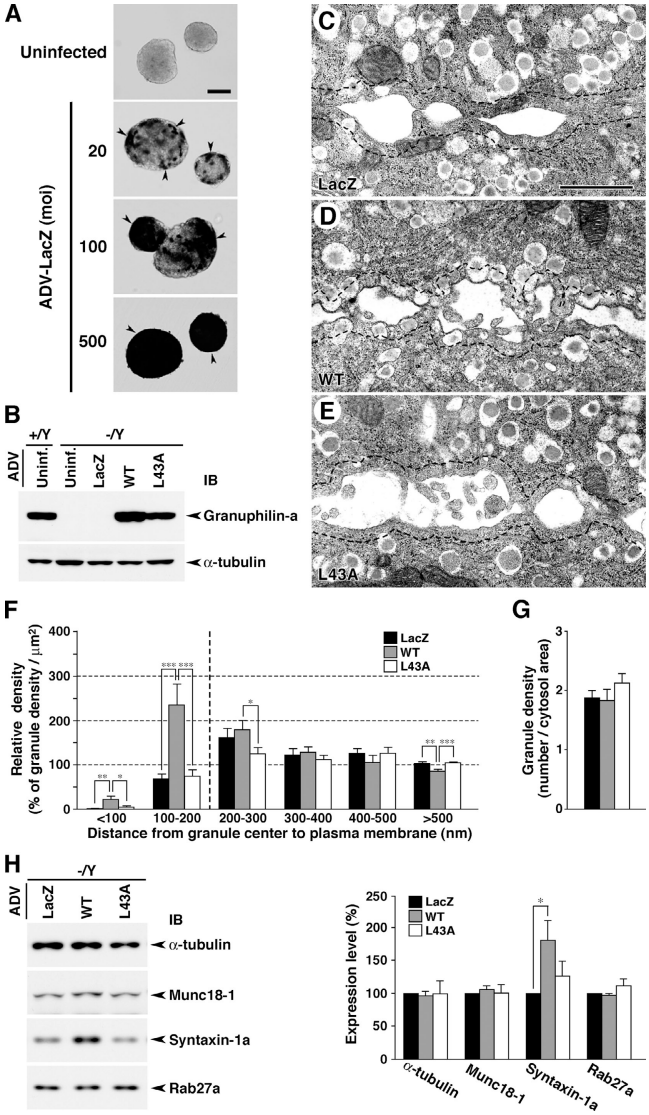

Figure 8. **Rescue of granuphilin-null β cell phenotypes by ADV-mediated granuphilin expression.** (A) ADV-mediated LacZ expression in isolated islets. The islets were infected with ADV-encoding LacZ at different MOI from 20 to 500 at 37°C for 2 h and then cultured in a fresh medium for 48 h. LacZ expression was visualized by X-gal substrate enzyme activity (dark-colored cells, arrowheads). Bar, 100 μm. (B) Expression levels of granuphilin-a in islets uninfected (Uninf.) or infected for 48 h with an ADV-encoding LacZ, wild-type (WT), or L43A mutant (L43A) granuphilin-a (MOI = 500). Protein expression levels were analyzed by immunoblotting (IB) with antigranuphilin αGrp-N and anti–α-tubulin antibodies. (C–E) Electron micrographs of β cell sections from ADV-infected $Grn^{-/Y}$ islets (MOI = 500). Dashed lines indicate borders 200 nm distant from the plasma membrane. Bar, 1 μm. (F and G) Morphometric analyses of insulin granules in electron micrographs of ADV-infected $Grn^{-/Y}$ β cell sections. Relative density of granules located near the plasma membrane (F) and average granule number per cytosol area (μm²; G) were calculated as in Fig. 5 (C and D) from 12 randomly selected β cells of each group that had been infected with ADV-encoding LacZ, WT, or L43A. *, $P < 0.05$; **, $P < 0.01$; ***, $P < 0.005$. (H) Immunoblot analysis of ADV-infected islets. Total protein was extracted at 48 h after ADV infection and reacted with the antibodies indicated (left). Protein expression levels were quantified from six preparations (right). *, $P = 0.027$. Results are provided as mean ± SEM.

tion (MOI) <100, the higher titers at MOI 250–500 achieved overall expression and thus were used for the rescue experiments. Infection of the mutant islets with ADV-encoding wild-type granuphilin-a induced a protein level equivalent to the endogenous level in uninfected wild-type islets (Fig. 8 B and Fig. S1). Moreover, it restored morphologically docked granules in the mutant β cells, in contrast to the expression of control LacZ (Fig. 8, C, D, and F). The relative density of granules near the plasma membrane in granuphilin-a–expressed mutant cells was comparable with that observed in noninfected wild-type β cells (Fig. 8 F vs. Fig. 5 C). The granule density, however, was reduced in infected β cells compared with uninfected β cells (Fig. 8 G vs. Fig. 5 D), a result that occurred irrespective of the expressed protein and could be ascribed to the background effect of the virus infection. Because of this effect, we did not examine the effect on insulin secretion, although we suspect that granuphilin expression decreases the evoked insulin secretion as was reported in MIN6 cells (Torii et al., 2002). Importantly, the restoration of morphologically docked granules was not seen by the expression of the granuphilin-a mutant L43A, which is specifically defective in binding to syntaxin-1a (Torii et al., 2002; Fig. 8, E and F). The differential effect should be specific to the protein expressed because it was observed in cells close to the outer margin of the islets, where infection occurs most efficiently (unpublished data), and because we infected the islets under conditions in which almost all cells express exogenous proteins (Fig. 8 A). Consistently, we previously demonstrated that the overexpression of the L43A mutant in MIN6 cells fails to promote the targeting of insulin granules onto the plasma membrane or to inhibit high K^+-induced insulin secretion efficiently, in contrast to the case of the wild type (Torii et al., 2002, 2004). Besides the effect on granule docking, the expression of wild-type granuphilin-a, but not of the L43 mutant, significantly increased the protein level of syntaxin-1a (Fig. 8 H). By contrast, the expression of granuphilin-a did not alter the protein level of Munc18-1. These findings suggest that the reductions in docked granules and syntaxin-1a expression are direct consequences of granuphilin deficiency, whereas the decreased level of Munc18-1 is a secondary phenomenon resulting from the chronic deficiency in granuphilin and/or syntaxin-1a.

Discussion

We demonstrate that granuphilin is a principal docking factor for insulin granules. Residually docked granules observed in granuphilin-null β cells likely correspond to those stochastically located close to the plasma membrane, given the high density and diffuse distribution of granules in the cytoplasm. Surprisingly, despite the docking defect, evoked exocytosis is significantly increased in the mutant cells, indicating that granuphilin plays a negative regulatory role in insulin secretion. The seemingly contradictory phenotypes were initially unexpected but are completely consistent with our previous findings that the overexpression of granuphilin promotes a peripheral redistribution of insulin granules and reduces the evoked insulin secretion in MIN6 cells (Torii et al., 2002, 2004). These findings indicate that stable and tight docking is not an absolute prerequisite for fusion and that the releasable vesicles may not necessarily be located close to the exocytotic site. Past studies

with evanescent wave microscopy have indicated that immobile docked granules primarily participate in the initial phase of exocytosis in chromaffin cells (Steyer et al., 1997) and MIN6 cells (Ohara-Imaizumi et al., 2002). Although these findings may hold true for an immediately releasable pool, they do not mean that stable predocking is required for fusion. In fact, a substantial release from newly recruited granules has been observed in both the early and late phases of glucose-induced insulin secretion in normal mouse pancreatic β cells (Kasai et al., 2005). Further, it has been shown that extensively mobile undocked granules support exocytosis more efficiently than immobile docked ones at growth cones in PC12 cells and hippocampal neurons (Han et al., 1999; Silverman et al., 2005). Furthermore, despite the much faster time scale for the release of synaptic vesicles compared with secretory granules, the release-competent vesicles that are recycled at the frog neuromuscular junction are dispersed randomly throughout the terminal (Rizzoli and Betz, 2004). These findings are consistent with the view that the release-competent secretory vesicles do not necessarily lie within the morphologically docked vesicles.

Because granuphilin has bilateral roles in promoting docking and in inhibiting a subsequent fusion of granules, we suggest that the docking machinery in regulated exocytosis imposes a constraint on stimulus-evoked fusion. Torii et al. (2002) showed that granuphilin exclusively interacts with a fusion-incompetent, closed form of syntaxin-1a. In the present study, we demonstrated that granuphilin is an essential molecule both for the preservation of the expression levels of syntaxin-1a and Munc18-1 and for the maintenance of the syntaxin-1a–Munc18-1 complex formation. The rescue experiment in granuphilin-null cells further showed that the ability of granuphilin to interact with syntaxin-1a is required for its docking activity, although another mechanism may contribute to the docking process, such as to the binding to membrane lipids through its COOH-terminal C2 domains (Wang et al., 1999). These findings indicate that granuphilin stabilizes syntaxin-1a in a fusion-incompetent, closed form during the docking process. Munc18-1 may also participate in the granuphilin-mediated docking process because it has an affinity to both granuphilin (Coppola et al., 2002; unpublished data) and the closed form of syntaxin-1a (Dulubova et al., 1999; Misura et al., 2000; Yang et al., 2000). In fact, Munc18-1 has been shown to play a role in the docking of chromaffin granules and synaptic vesicles (Voets et al., 2001; Weimer et al., 2003). Genetic and physical interactions between Rab effectors and Sec1/Munc18 proteins have been well documented in other transport pathways (Segev, 2001). Based on these findings, we propose that granuphilin mediates the docking of granules by using the syntaxin-1a–Munc18-1 complex as a recognition platform at the plasma membrane, although it is unclear whether granuphilin forms a complex with syntaxin-1a and Munc18-1 simultaneously or separately in vivo. These docking protein complexes, unless disassembled, should inhibit membrane fusion by preventing syntaxin-1a from forming a core complex with other SNARE proteins. On this assumption, a decreased formation of the syntaxin-1a–Munc18-1 complex will lead to enhanced stimulus-evoked secretion, as was observed in the granuphilin-null β cells. The bilateral nature of docking machinery explains why the overexpression of these proteins often shows inhibitory effects on secretion despite their putatively positive roles for the docking and fusion processes (Schulze et al., 1994; Nagamatsu et al., 1996; Dresbach et al., 1998; Zhang et al., 2000; Coppola et al., 2002; Torii et al., 2002). It may also explain why the mode of interaction between Sec1/Munc18 proteins and syntaxins is specialized in regulated exocytosis (Rizo and Südhof, 2002). The enhanced exocytosis, however, is unique in granuphilin-deficient cells in contrast to the null or reduced exocytosis in syntaxin-1a– or Munc18-1–deficient cells (Schulze et al., 1995; Verhage et al., 2000; Voets et al., 2001). The difference suggests that granuphilin is a genuine docking factor, whereas syntaxin-1a and Munc18-1 have additional postdocking roles as indicated previously (Rizo and Südhof, 2002).

Rab27a and granuphilin physiologically interact with each other in pancreatic β cells because the two proteins colocalize intracellularly (Yi et al., 2002), are redistributed in the absence of the other protein (Kasai et al., 2005; this study), and form the endogenous complex (Yi et al., 2002; this study). Granuphilin-null β cells, however, exhibit markedly more severe ultrastructural changes in the docking pattern of granules than do *ashen* β cells that lack functional Rab27a, although *ashen* β cells show impairment in replenishing docked granules during glucose stimulation (Kasai et al., 2005). We previously thought that it might be difficult to recapture the docking state of secretory granules by conventional electron microscopy without rapid freezing techniques. It is now clear that there are marked differences in the docking state in chemically fixed β cells between the two mutants. In addition, *ashen* β cells exhibit decreased insulin secretion in response to high glucose levels (Kasai et al., 2005), in contrast to granuphilin-null β cells but consistent with the finding that the overexpressed Rab27a augments evoked insulin secretion in MIN6 cells (Yi et al., 2002). The differential effects on granule docking and exocytosis of Rab27a and granuphilin, whether eliminated or overexpressed, suggest that the functional relationship of these two proteins in β cells is not as simple as Rab27a and its other effector melanophilin in melanocytes, where their mutations cause similar, if not identical, defects in the transport of melanosomes (Wilson et al., 2000; Matesic et al., 2001). Compensation for Rab27a deficiency by Rab3a is possible but should be limited because the amount of endogenous complex between Rab3a and granuphilin, which can be faintly detected in wild-type islets, was not increased in *ashen* islets (unpublished data). The activity cycle of Rab27a may only have a regulatory role in granule exocytosis, such as in promoting the disassembly of the fusion-incompetent syntaxin-1a–Munc18-1 complex in the presence of a high glucose concentration. Another possibility is that the mutant phenotypes are modulated by the presence of other Rab27a-binding proteins (Izumi et al., 2003), whose function may be lost in *ashen* β cells but are ectopically gained by artificial binding to Rab27a in the absence of granuphilin. Although these possibilities need to be clarified in the future, the severe impairment in docking in granuphilin-null cells and its ready restoration by granuphilin expression indicate that granuphilin plays a direct and physical role in the docking process.

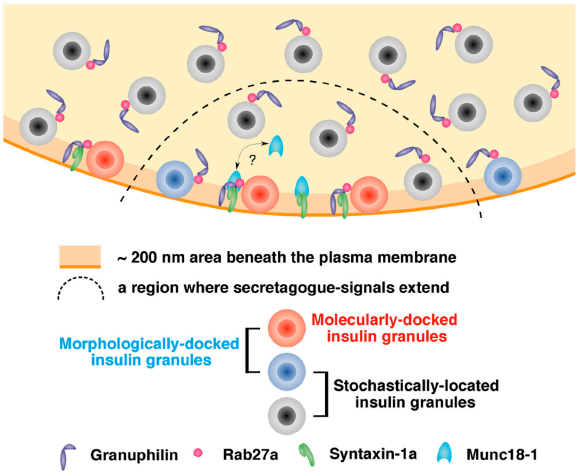

Figure 9. **Schematic model for docked granules.** Morphologically docked granules, whose centers reside within 200 nm of the plasma membrane in this figure, consist of molecularly docked granules (red) and those just stochastically located close to the plasma membrane (blue). Granuphilin links insulin granules to the fusion-incompetent, closed form of syntaxin-1a, although it is currently unknown whether it interacts with free syntaxin-1a or the syntaxin-1a–Munc18-1 complex. Such molecularly docked granules need to be primed for fusion. The priming reaction somehow disassembles the docking protein complex and enables syntaxin-1a to adopt an open configuration and thus to form a complex with other SNARE proteins. In response to a secretory stimulus, primed molecularly docked granules (some of the red granules), molecularly undocked but morphologically docked granules (blue), and even undocked granules (black) can be released from a region where secretagogue-dependent signals extend (inside of the dashed line). Although there are no molecularly docked granules (red), evoked exocytosis is augmented in granuphilin-deficient cells, indicating that molecular docking is inhibitory for fusion.

In summary, we demonstrated increased evoked exocytosis despite a severely reduced docking of insulin granules in granuphilin-deficient pancreatic β cells. The existence of a predocked vesicle pool is a hallmark of regulated exocytosis, in which constitutive fusion of incoming vesicles is inhibited. The prevailing view has been that a readily releasable pool of vesicles resides within the docked pool that has been primed (Burgoyne and Morgan, 2003; Rorsman and Renström, 2003), although the definition of the pool is often vague, especially in the case of secretory granules, whose release has a relatively slow onset and extends over a relatively long time scale. Our model is schematically shown in Fig. 9, which demonstrates that morphologically docked granules are composed of heterogeneous populations: those just stochastically located close to the membrane and those molecularly docked to the fusion machinery. The docking machinery in regulated exocytosis not only promotes vesicles in apposition to the plasma membrane but simultaneously imposes a temporal constraint to inhibit subsequent fusion. The priming reaction, which is also unique to regulated exocytosis, may be only rate limiting for molecularly docked vesicles to release the docking constraint. Thus, a readily, if not immediately, releasable pool cannot be defined morphologically. Besides imposing the need for priming on docked vesicles, docking occupies a part of the fusion machinery and thereby may further restrict the fusion of incoming undocked vesicles. As such, docking likely contributes to the fine-tuning of secretion in response to external stimuli. Finally, the presence of enhanced glucose tolerance in granuphilin-null mice suggests that the modification of granuphilin function should be explored as a novel pharmaceutical target strategy for the treatment of diabetes.

Materials and methods

Generation of granuphilin-deficient mice

The genomic DNA clones of mouse *Grn* were isolated from a 129/Sv genomic library by screening with a mouse cDNA fragment (Wang et al., 1999). The targeting vector was constructed with an 8.6-kb fragment that spans from intron 1 to intron 2 as a 5′ homologous region, a 5.0-kb fragment from exon 5 to intron 5 as a 3′ homologous region, a floxed pgk-neo fragment (a gift from M. Rudnicki, The Ottawa Health Research Institute, Ottawa, Canada; McBurney et al., 1991), and a DTA gene cassette (a gift from S. Aizawa, RIKEN Center for Developmental Biology, Kobe, Japan; Yagi et al., 1990). Culture of embryonic stem cell E14 (a gift from M. Hooper, Western General Hospital, Edinburgh, UK; Hooper et al., 1987) and targeting experiments were performed as described previously (Gomi et al., 1995). Homologous recombinants were identified by Southern hybridization of the genomic DNA. The embryonic stem cell clones containing the targeting event were microinjected into C57BL/6J blastocysts to generate chimeric mice. Mice heterozygous for the targeted allele in the female ($Grn^{+/-}$) were obtained by crossing the male chimeras with female C3H/He mice ($Grn^{+/+}$). Mutant lines were maintained as female heterozygotes by backcrossing with C3H/He mice. Wild-type ($Grn^{+/Y}$) and knockout ($Grn^{-/Y}$) males for the experiments were also obtained by backcrossing. Genotype analysis was done by Southern hybridization and/or PCR. The primers designed for the exon 4/exon 5 boundary region of *Grn* and pgk-neo were as follows: *Grn/Fow1*, 5′-ACAGGCAGCGAGATAATCAG-3′; *Grn/Rev1*, 5′-TGAATGATCCTTCTTCCTGG-3′; and *Neo/Fow2*, 5′-CTTGACGAGTTCTTCTGAGG-3′. Mice had free access to water and standard laboratory chow (CE-2; CLEA Japan) in an air-conditioned room with a 12-h light–dark cycle. All animal experiments were conducted according to the guidelines of the Animal Care and Experimentation Committee, Gunma University, Showa Campus, Japan.

Glucose tolerance test, insulin tolerance test, and measurement of insulin

An i.p. glucose tolerance test (1 g glucose/kg body weight) and an i.p. insulin tolerance test (0.75 U human insulin/kg body weight) were performed as described previously (Kasai et al., 2005). The plasma insulin concentration was measured with an LBIS mouse insulin ELISA kit (U-type; Shibayagi). For the measurement of insulin content, the excised pancreata were cut into small pieces, homogenized using a glass-Teflon homogenizer (2,000 rpm, 25 strokes) in an acid-ethanol solution (0.18 N HCl-70% ethanol), and sonicated three times for 15 s each. After centrifugation at 10,000 *g* for 10 min, the immunoreactive insulin in the supernatant was measured with an insulin radioimmunoassay kit (Eiken Chemical).

Perifusion insulin secretion assay

Islets were isolated from cervically dislocated mice by pancreatic duct injection of 500 U/ml of collagenase solution (type XI; Sigma-Aldrich) followed by digestion at 37°C for 30 min with mild shaking, as described previously (Kasai et al., 2005). The isolated islets were cultured overnight in RPMI 1640 medium supplemented with 10% FCS. 30 islets were perifused with LG Krebs-Ringer buffer (10 mM Hepes, pH 7.4, 118.4 mM NaCl, 4.7 mM KCl, 1.9 mM $CaCl_2$, 1.3 mM $MgSO_4$, 1.2 mM KH_2PO_4, 25 mM $NaHCO_3$, 0.1% BSA, and 2.8 mM glucose) at a constant flow rate of 1.0 ml/min for 30 min. After this stabilization period, they were further perifused with the same buffer for 10 min followed by the buffer containing various secretagogues. Forskolin and phorbol-12-myristate-13-acetate were purchased from Sigma-Aldrich and Calbiochem, respectively. All of the perifusate solution was equilibrated with 95% O_2 and 5% CO_2 and maintained at 37°C. Fractions were collected every 1 min, and the secreted insulin was measured.

Immunoblot and immunoprecipitation

Levels of protein expression and interaction in the isolated islets were analyzed as described previously (Kasai et al., 2005). For coimmunoprecipitation analysis, protein extracts were incubated with 5 μl of rabbit anti-Munc18 serum (Synaptic Systems GmbH) or monoclonal anti-Rab3a or anti-Rab27a antibody (BD Biosciences) overnight at 4°C. Protein interactions of syntaxin-1a with Munc18-1 and granuphilin with Rab27a were analyzed by immunoblotting of the immune complexes. Chemiluminescent

signals on the x-ray film were captured with an image scanner (model CC-500L; Epson), and recorded images were quantified using Gel Plotting Macros of NIH Image 1.62 software.

Light microscopic analyses of pancreatic islet cells

For the analyses of islet size and β cell mass, paraffin-embedded pancreas sections (4 μm) were labeled with antiinsulin antibody and detected by an avidin-biotin-peroxidase technique (Vector Laboratories) with hematoxylin counter staining. Sections were collected at 400-μm intervals from tissue blocks, and all islets in the sections were analyzed in their size distribution and β cell mass (100× insulin-positive area/total islet area). Image acquisition and analysis were completed using a microscope (BX50; Olympus) equipped with a charge-coupled device camera (DP-70; Olympus) and ImageJ 1.31 software (http://rsb.info.nih.gov/nih-image/).

For immunohistochemistry, mice were fixed with 4% PFA in 0.1 M sodium phosphate buffer, pH 7.4, via cardiac perfusion. 20-μm-thick frozen sections were prepared on a 0.1% gelatin-coated slide glass by cryocut (Jung CM3000; Leica). The sections were permeabilized with 0.1% Triton X-100/PBS and blocked by incubation with 5% normal goat serum. Subsequently, the sections were reacted with rabbit antigranuphilin antibody, αGrp-N that recognizes both granuphilin-a and -b (Yi et al., 2002), rabbit antiglucagon antibody (Biogenesis), guinea pig antiinsulin antibody (a gift from H. Kobayashi, Gunma University, Maebashi, Japan), or monoclonal anti–HPC-1/syntaxin-1a/1b antibody (Sigma-Aldrich). The sections were then incubated with AlexaFluor-labeled secondary antibodies (Invitrogen). Immunofluorescence was viewed with a microscope (BX50; Olympus) with objective lens (100×; UplanApo) and a charge-coupled device camera (model SenSys; Photometrics). Immunofluorescent images were acquired using IPLab 3.2 software (Scanalytics), and the intensity was analyzed using ImageJ 1.31 software.

Primary culture of islet cells was performed as described previously (Wollheim et al., 1990), with minor modifications. In brief, 70–80 islets that had been cultured overnight were washed with PBS and digested with trypsin-EDTA (0.05%–0.53 mM) for 8 min at 37°C. After dispersion by pipetting, cells were seeded onto 12-mm glass-bottomed culture dishes (Iwaki Scitech) coated with 50 μg/ml poly-L-lysine (Nacalai Tesque) and cultured for 4–6 d. Cells were fixed with 4% PFA on ice for 30 min, permeabilized with 0.1% Triton X-100/PBS for 10 min, and immunostained.

EM

Electron microscopic analysis of docked granules was performed on the naive pancreatic islet tissues and on the isolated islets as described previously (Kasai et al., 2005). The pancreas was removed from mice and fixed by immersion shaking with 2% PFA/2.5% glutaraldehyde in 0.1 M sodium phosphate buffer, pH 7.4, for 4 h at RT. The isolated islets cultured overnight were preincubated with Krebs-Ringer buffer containing 2.8 mM glucose at 37°C for 1 h, and some of them were then stimulatory incubated with the buffer containing 25 mM glucose at 37°C for 30 min. Subsequently, the samples were fixed by immersion shaking with 2% PFA/2% glutaraldehyde/0.2% picric acid in 0.1 M cacodylate buffer, pH 7.4, for 1.5 h at RT. They were then regularly processed and examined with an electron microscope (JEM 1010; JEOL) at an acceleration voltage of 80 kV. The pictures (5,000× and 8,000×) were scanned and analyzed by ImageJ 1.31 software.

Infection of isolated islets with recombinant ADV

Mouse granuphilin-a wild type or L43A mutant was expressed in granuphilin-null islets by a recombinant ADV-expression system as described previously (Torii et al., 2002, 2004; Yi et al., 2002). *AxCALacZ*, which expresses bacterial LacZ, was used as a control ADV. Isolated islets were cultured overnight and selected by their size (100- to 250-μm diam) for virus infection. Approximately 60–80 islets were infected at 37°C for 2 h with the ADV vectors at 250–500 MOI, assuming 10^3 cells per islet on average. The infected islets were then transferred to the fresh medium and cultured for 48 h. The control *AxCALacZ*-infected islets were stained with 1 mg/ml x-gal substrate (Nacalai Tesque) at 37°C for 3 h as described previously (Gomi et al., 1995).

Statistical analysis

Results are given as the mean ± SEM, except where indicated otherwise. Differences between the means were assessed by *t* test. The amount of secreted insulin in perifusion assays was assessed by a repeated measure of an analysis of variance. Immunoblot signals were analyzed by a Wilcoxon signed-rank test.

Online supplemental material

Fig. S1 shows the entire images for immunoblots in Figs. 6–8. Online supplemental material is available at http://www.jcb.org/cgi/content/full/jcb.200505179/DC1.

We are grateful for technical assistance from T. Ishizaka for the morphometric analyses; from Y. Onodera, A. Okada, and Y. Saito for the embryonic stem cell injection; and from H. Takemura and N. Satoh for the mouse colony maintenance.

This work was supported by grants-in-aid for scientific research (15079201, 16390261, and 17659272) and the 21st Century Center of Excellence Program from the Ministry of Education, Culture, Sports, Science and Technology of Japan, and in part by grants from Daiwa Securities Health Foundation and Novo Nordisk Insulin Study Award (to T. Izumi).

Submitted: 31 May 2005
Accepted: 6 September 2005

References

Burgess, T.L., and R.B. Kelly. 1987. Constitutive and regulated secretion of proteins. *Annu. Rev. Cell Biol.* 3:243–293.

Burgoyne, R.D., and A. Morgan. 2003. Secretory granule exocytosis. *Physiol. Rev.* 83:581–632.

Coppola, T., C. Fantz, V. Perret-Menoud, S. Gattesco, H. Hirling, and R. Regazzi. 2002. Pancreatic β-cell protein granuphilin binds Rab3 and Munc-18 and controls exocytosis. *Mol. Biol. Cell.* 13:1906–1915.

Dresbach, T., M.E. Burns, V. O'Connor, W.M. DeBello, H. Betz, and G.J. Augustine. 1998. A neuronal Sec1 homolog regulates neurotransmitter release at the squid giant synapse. *J. Neurosci.* 18:2923–2932.

Dulubova, I., S. Sugita, S. Hill, M. Hosaka, I. Fernandez, T.C. Südhof, and J. Rizo. 1999. A conformational switch in syntaxin during exocytosis: role of munc18. *EMBO J.* 18:4372–4382.

Gomi, H., T. Yokoyama, K. Fujimoto, T. Ikeda, A. Katoh, T. Itoh, and S. Itohara. 1995. Mice devoid of the glial fibrillary acidic protein develop normally and are susceptible to scrapie prions. *Neuron.* 14:29–41.

Han, W., Y.-K. Ng, D. Axelrod, and E.S. Levitan. 1999. Neuropeptide release by efficient recruitment of diffusing cytoplasmic secretory vesicles. *Proc. Natl. Acad. Sci. USA.* 96:14577–14582.

Hooper, M., K. Hardy, A. Handyside, S. Hunter, and M. Monk. 1987. HIPRT-deficient (Lesch-Nyhan) mouse embryos derived from germline colonization by cultured cells. *Nature.* 326:292–295.

Izumi, T., H. Gomi, K. Kasai, S. Mizutani, and S. Torii. 2003. The roles of Rab27 and its effectors in the regulated secretory pathways. *Cell Struct. Funct.* 28:465–474.

Johns, L.M., E.S. Levitan, E.A. Shelden, R.W. Holz, and D. Axelrod. 2001. Restriction of secretory granule motion near the plasma membrane of chromaffin cells. *J. Cell Biol.* 153:177–190.

Kasai, K., M. Ohara-Imaizumi, N. Takahashi, S. Mizutani, S. Zhao, T. Kikuta, H. Kasai, S. Nagamatsu, H. Gomi, and T. Izumi. 2005. Rab27a mediates the tight docking of insulin granules onto the plasma membrane during glucose stimulation. *J. Clin. Invest.* 115:388–396.

Matesic, L.E., R. Yip, A.E. Reuss, D.A. Swing, T.N. O'Sullivan, C.F. Fletcher, N.G. Copeland, and N.A. Jenkins. 2001. Mutations in *Mlph*, encoding a member of the Rab effector family, cause the melanosome transport defects observed in *leaden* mice. *Proc. Natl. Acad. Sci. USA.* 98:10238–10243.

McBurney, M.W., L.C. Sutherland, C.N. Adra, B. Leclair, M.A. Rudnicki, and K. Jardine. 1991. The mouse Pgk-1 gene promoter contains an upstream activator sequence. *Nucleic Acids Res.* 19:5755–5761.

Misura, K.M.S., R.H. Scheller, and W.I. Weis. 2000. Three-dimensional structure of the neuronal-Sec1–syntaxin 1a complex. *Nature.* 404:355–362.

Nagamatsu, S., T. Fujiwara, Y. Nakamichi, T. Watanabe, H. Katahira, H. Sawa, and K. Akagawa. 1996. Expression and functional role of syntaxin 1/HPC-1 in pancreatic β cells: syntaxin 1A, but not 1B, plays a negative role in regulatory insulin release pathway. *J. Biol. Chem.* 271:1160–1165.

Ohara-Imaizumi, M., Y. Nakamichi, T. Tanaka, H. Ishida, and S. Nagamatsu. 2002. Imaging exocytosis of single insulin secretory granules with evanescent wave microscopy: distinct behavior of granule motion in biphasic insulin release. *J. Biol. Chem.* 277:3805–3808.

Rizo, J., and T.C. Südhof. 2002. SNAREs and Munc18 in synaptic vesicle fusion. *Nat. Rev. Neurosci.* 3:641–653.

Rizzoli, S.O., and W.J. Betz. 2004. The structural organization of the readily releasable pool of synaptic vesicles. *Science.* 303:2037–2039.

Rizzoli, S.O., and W.J. Betz. 2005. Synaptic vesicle pools. *Nat. Rev. Neurosci.* 6:57–69.

Rorsman, P., and E. Renström. 2003. Insulin granule dynamics in pancreatic beta cells. *Diabetologia.* 46:1029–1045.

Schulze, K.L., J.T. Littleton, A. Salzberg, N. Halachmi, M. Stern, Z. Lev, and H.J. Bellen. 1994. rop, a *Drosophila* homolog of yeast Sec1 and vertebrate n-Sec1/Munc18 proteins, is a negative regulator of neurotransmitter release in vivo. *Neuron.* 13:1099–1108.

Schulze, K.L., K. Broadie, M.S. Perin, and H.J. Bellen. 1995. Genetic and electrophysiological studies of *Drosophila* syntaxin-1A demonstrate its role in nonneuronal secretion and neurotransmission. *Cell.* 80:311–320.

Segev, N. 2001. Ypt and Rab GTPases: insight into functions through novel interactions. *Curr. Opin. Cell Biol.* 13:500–511.

Serano, J., and G.M. Rubin. 2003. The *Drosophila* synaptotagmin-like protein bitesize is required for growth and has mRNA localization sequences within its open reading frame. *Proc. Natl. Acad. Sci. USA.* 100:13368–13373.

Silverman, M.A., S. Johnson, D. Gurkins, M. Farmer, J.E. Lochner, P. Roa, and B.A. Scalettar. 2005. Mechanisms of transport and exocytosis of dense-core granules containing tissue plasminogen activator in developing hippocampal neurons. *J. Neurosci.* 25:3095–3106.

Steyer, J.A., H. Horstmann, and W. Almers. 1997. Transport, docking and exocytosis of single secretory granules in live chromaffin cells. *Nature.* 388:474–478.

Torii, S., S. Zhao, Z. Yi, T. Takeuchi, and T. Izumi. 2002. Granuphilin modulates the exocytosis of secretory granules through interaction with syntaxin 1a. *Mol. Cell. Biol.* 22:5518–5526.

Torii, S., T. Takeuchi, S. Nagamatsu, and T. Izumi. 2004. Rab27 effector granuphilin promotes the plasma membrane targeting of insulin granules via interaction with syntaxin 1a. *J. Biol. Chem.* 279:22532–22538.

Verhage, M., A.S. Maia, J.J. Plomp, A.B. Brussaard, J.H. Heeroma, H. Vermeer, R.F. Toonen, R.E. Hammer, T.K. van den Berg, M. Missler, et al. 2000. Synaptic assembly of the brain in the absence of neurotransmitter secretion. *Science.* 287:864–869.

Voets, T., R.F. Toonen, E.C. Brian, H. de Wit, T. Moser, J. Rettig, T.C. Südhof, E. Neher, and M. Verhage. 2001. Munc18-1 promotes large dense-core vesicle docking. *Neuron.* 31:581–591.

Wang, J., T. Takeuchi, H. Yokota, and T. Izumi. 1999. Novel rabphilin-3-like protein associates with insulin-containing granules in pancreatic beta cells. *J. Biol. Chem.* 274:28542–28548.

Weimer, R.M., J.E. Richmond, W.S. Davis, G. Hadwiger, M.L. Nonet, and E.M. Jorgensen. 2003. Defects in synaptic vesicle docking in *unc-18* mutants. *Nat. Neurosci.* 6:1023–1030.

Wilson, S.M., R. Yip, D.A. Swing, T.N. O'Sullivan, Y. Zhang, E.K. Novak, R.T. Swank, L.B. Russell, N.G. Copeland, and N.A. Jenkins. 2000. A mutation in *Rab27A* causes the vesicle transport defects observed in *ashen* mice. *Proc. Natl. Acad. Sci. USA.* 97:7933–7938.

Wollheim, C.B., P. Meda, and P.A. Halban. 1990. Isolation of pancreatic islets and primary culture of the intact microorgans or of dispersed islet cells. *Methods Enzymol.* 192:188–223.

Yagi, T., Y. Ikawa, K. Yoshida, Y. Shigetani, N. Takeda, I. Mabuchi, T. Yamamoto, and S. Aizawa. 1990. Homologous recombination at c-*fyn* locus of mouse embryonic stem cells with use of diphtheria toxin A-fragment gene in negative selection. *Proc. Natl. Acad. Sci. USA.* 87:9918–9922.

Yang, B., M. Steegmaier, L.C. Gonzalez, and R.H. Scheller. 2000. nSec1 binds a closed conformation of syntaxin1A. *J. Cell Biol.* 148:247–252.

Yi, Z., H. Yokota, S. Torii, T. Aoki, M. Hosaka, S. Zhao, K. Takata, T. Takeuchi, and T. Izumi. 2002. The Rab27a/granuphilin complex regulates the exocytosis of insulin-containing dense-core granules. *Mol. Cell. Biol.* 22:1858–1867.

Zhang, W., A. Efanov, S.-N. Yang, G. Fried, S. Kölare, H. Brown, S. Zaitsev, P.-O. Berggren, and B. Meister. 2000. Munc-18 associates with syntaxin and serves as a negative regulator of exocytosis in the pancreatic β-cell. *J. Biol. Chem.* 275:41521–41527.